Journal of Engineering Science and Technology
Vol. 12, No. 11 (2017) 3011 - 3022

BOUNDARY LAYER AND AMPLIFIED GRID EFFECTS ON AERODYNAMIC PERFORMANCES OF S809 AIRFOIL FOR HORIZONTAL AXIS WIND TURBINE (HAWT)

YOUNES EL KHCHINE*, MOHAMMED SRITI

Engineering Sciences Laboratory, Polydisciplinary Faculty of Taza,
Sidi Mohamed Ben Abdellah University, Road of Oujda – B.P. 1223, Taza, Morocco.
* Corresponding Author: younes.elkhchine@usmba.ac.ma

Abstract

The design of rotor blades has a great effect on the aerodynamics performances of horizontal axis wind turbine and its efficiency. This work presents the effects of mesh refinement and boundary layer on aerodynamic performances of wind turbine S809 rotor. Furthermore, the simulation of fluid flow is taken for S809 airfoil wind turbine blade using ANSYS/FLUENT software. The problem is solved by the conservation of mass and momentum equations for unsteady and incompressible flow using advanced SST k-ω turbulence model, in order to predict the effects of mesh refinement and boundary layer on aerodynamics performances. Lift and drag coefficients are the most important parameters in studying the wind turbine performance, these coefficients are calculated for four meshes refinement and different angles of attacks with Reynolds number is 10^6. The study is applied to S809 airfoil which has 21% thickness, specially designed by NREL for horizontal axis wind turbines.

Keywords: S809 airfoil, Aerodynamic performances, CFD Simulation, SST k-ω turbulence model, Boundary layer.

1. Introduction

The computational fluid dynamics (CFD) approach is the most appropriate method to investigate the mechanical power of wind turbine, this approach provides a best description of flow around wind turbine rotor, and gives a detailed description of turbulence phenomenon. With the increasing computing capacity, the CFD approach is becoming a practical tool to model and simulate the aerodynamic performances of wind turbine in three-dimensional.

Nomenclatures

c	Chord length, m
D_h	Hydraulic diameter, m
k	Turbulent kinetic energy, m^2/s^2
p	Pressure, Pa
Re	Reynolds number
u^*	Friction velocity, m/s
V_∞	Velocity of fluid, m/s
y^+	Dimensionless wall
y_0	Wall distance, m

Greek Symbols

α	Angle of attack, °
β	Twist angle, °
μ	Dynamic viscosity, kg/m.s
ν	Kinematic viscosity, m^2/s
ρ	Density, kg/m^3
τ	Stress tensor, Pa
ω	Turbulence dissipation energy rate, m^2/s^3

Abbreviations

CFD	Computational Fluid Dynamics
DUT	Delft University of Technology
NREL	National Renewable Energy Laboratory
RANS	Reynolds Averaged Navier-Stokes
SST	Shear Stress Transport

Although many studies have been published on the subject of horizontal-axis wind turbine blades CFD simulation, which are the effects of mesh refinement and adaptive grids on the aerodynamic performances over NACA 0012 airfoil [1, 2]. This simulation based on the Reynolds Averaged Navier-Stokes equations using finite volume method with a range of meshes.

The roughness effects on aerodynamic characteristics of a wind turbine airfoil. is performed by numerical simulation of the turbulent flow around airfoil with a resolution the Reynolds Averaged Navier-Stokes equations (RANS) with k-ε turbulence model using quadrilateral structured mesh [3]. The mesh is very fine near of airfoil surface to satisfy the turbulence model conditions and in order to predict the nature of flows, pressure and velocity gradient around airfoil surface. The simulation was made for a rough and smooth profile to investigate the effects of the roughness characteristics of airfoil.

The near wall grid spacing investigations for the SST k-ω turbulence model was studied for aerodynamic behaviour of horizontal axis wind turbine [4]. Eight different cases were investigated for the near wall grid spacing and all cases which the total number of nodes is fewer than 5000000.

An experimental study was performed of aerodynamic performances investigation of a NACA 2415 airfoil by varying attack angles at low Reynolds number. This study showed that as the angle of attack increased, the separation and the transition points moved towards the leading edge at all Reynolds number.

Furthermore, as the Reynolds number increased, stall characteristic changed and the mild stall occurred at higher Reynolds numbers whereas the abrupt stall occurred at lower Reynolds numbers [5].

Three models for predicting flow transition implemented in a 2D curvilinear, aerodynamic Navier–Stokes CFD code. These are Michel's empirical model, the eN model, and a newly proposed transition model (k–V model) [6]. The effect of the transition models on the airfoil aerodynamic characteristics at different Reynolds number and incidence angle are studied numerically. Both these parameters, when increased, promote the growth of flow perturbations. The test case is a 2D incompressible, low turbulence air flow around a smooth NACA0012 airfoil.

The effects of turbulence models on aerodynamic performances of the S809 and NACA 0012 airfoils developed by NREL were studied [7-10]. The flow modelled using unsteady incompressible Reynolds Averaged Navier-Stokes equations using different turbulence models to close the RANS equations with adaptive mesh refinement. The fluid flow simulated at different attack angles. Lift and drag coefficients calculated at each angle of attack. The performance of different turbulence models compared, and the results show that the best results given by SST k-ω of Menter turbulence model.

A new study of 2D numerical simulation of the steady low-speed flow for S-series wind-turbine-blade profiles, using Computational Fluid Dynamics (CFD) method based on the finite-volume approach [11]. The flow is governed by the Reynolds-Averaged-Navier-Stokes (RANS) equations. The main objective is to extract the lift and drag forces at each section of airfoil, and to determinate the slide ration (L/D) for each blade profile and at different wind speed. The optimum angle of attack for each blade profile is determined at the different wind speeds, the numerical results are benchmarked against wind tunnel measurements.

In this work, an extended analysis to perform 2D simulation of S809 wind turbine rotor is presented and discussed. The S809 airfoil is used in the turbine, which has 21% thickness with a sharp trailing edged and is designed specifically for HAWT and tested airfoil in high quality wind tunnels and the airfoil aerodynamic data are available in literature. The two-dimensional simulation of boundary layer and mesh refinement effects is performed. Different structured mesh size is studied by applying different number of nodes at the normal and tangential directions around the S809 airfoil. In all cases of simulations, the problem was described by the Reynolds Averaged Navier-Stokes equations combined with SST k-ω turbulence model of Menter [12] in order to enclose the boundary layer. Lift, drag and power are the most important parameters in studying the wind turbine performance. These coefficients are calculated for different meshes size and angles of attack. The simulation gives the accurate results compared with those presented by wind tunnel experiments of Delft University of Technology (DUT).

2. Mathematical Formulation and Turbulence Model

The wind flows around the airfoil described by solving the Navier-Stokes equations for unsteady and incompressible flow, the governing equations can be written as:

$$\frac{\partial u_j}{\partial x_j} = 0 \tag{1}$$

$$\frac{\partial u_i}{\partial t} + u_j \frac{\partial u_i}{\partial x_j} = -\frac{1}{\rho}\frac{\partial p}{\partial x_i} + \upsilon \frac{\partial}{\partial x_j}\left(\frac{\partial u_i}{\partial x_j} + \frac{\partial u_j}{\partial x_i}\right) + f_i \tag{2}$$

where u is the velocity, p is the pressure, t is the time, i and j are the directional components, ρ is the fluid density, υ is the kinematic viscosity and f_i are the external body forces.

For the 2D, unsteady and incompressible flow, the continuity equation for section of airfoil as shown in Fig. 1 is obtained by:

$$\frac{\partial u}{\partial x} + \frac{\partial v}{\partial y} = 0 \tag{3}$$

Momentum equations for viscous flow over airfoil section in x and y directions as shown in Fig. 1 are, respectively:

$$\frac{\partial u}{\partial t} + u\frac{\partial u}{\partial x} + v\frac{\partial v}{\partial y} = -\frac{1}{\rho}\frac{\partial p}{\partial x} + \upsilon\left(\frac{\partial^2 u}{\partial x^2} + \frac{\partial^2 v}{\partial y^2}\right) \tag{4}$$

$$\frac{\partial v}{\partial t} + u\frac{\partial v}{\partial x} + v\frac{\partial v}{\partial y} = -\frac{1}{\rho}\frac{\partial p}{\partial x} + \upsilon\left(\frac{\partial^2 v}{\partial x^2} + \frac{\partial^2 v}{\partial y^2}\right) \tag{5}$$

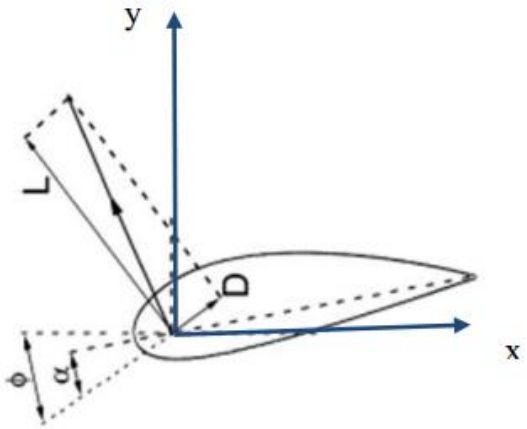

Fig. 1. Geometric parameters of airfoil section.

To account the turbulence effects, the instantaneous Navier-Stokes equations are averaged, this later is based on statistical approach applied on variables flow and decomposes velocity into an average and a fluctuation components $\bar{u}$ and u' respectively. The methodology applied is to solve the Reynolds Averaged Navier-Stokes equations RANS in two-dimensional for unsteady-state incompressible flow. The method of Reynolds is to decompose each physical variable in an average value and a fluctuating value:

$$u = \bar{u} + u'$$

$$v = \bar{v} + v'$$

$$p = \bar{p} + p'$$

Replacing the Reynolds decomposition in the continuity and momentum equations, we obtained the Reynolds Averaged Navier-Stokes equations (RANS) which are given in Eqs. (6) and (7):

$$\rho\frac{\partial \bar{u}}{\partial t} + \rho(\bar{u}\frac{\partial \bar{u}}{\partial x} + \bar{v}\frac{\partial \bar{u}}{\partial y}) = -\frac{\partial \bar{p}}{\partial x} + \mu(\frac{\partial^2 \bar{u}}{\partial x^2} + \frac{\partial^2 \bar{u}}{\partial y^2}) - \rho(\frac{\overline{\partial u' u'}}{\partial x} + \frac{\overline{\partial v' u'}}{\partial y}) \quad (6)$$

$$\rho\frac{\partial \bar{v}}{\partial t} + \rho(\bar{u}\frac{\partial \bar{v}}{\partial x} + \bar{v}\frac{\partial \bar{v}}{\partial y}) = -\frac{\partial \bar{p}}{\partial y} + \mu(\frac{\partial^2 \bar{v}}{\partial x^2} + \frac{\partial^2 \bar{v}}{\partial y^2}) - \rho(\frac{\overline{\partial v' v'}}{\partial x} + \frac{\overline{\partial v' u'}}{\partial y}) \quad (7)$$

with $-\rho\overline{u'v'}$ is the turbulent shear stress

The closure of the governing equations is based primarily on modelling fluctuating terms trained by additional variables *u'* and *v'*. Therefore, we used the SST *k*-ω turbulence model proposed by Menter [12] in 1993, this model used near the wall but switches to a *k*-ε model away from the wall. It's obtained from a combination of *k*-ω and *k*-ε models. This last, the most used; is a model for two equations, it provides the turbulent length scale in the near-wall region. By against the *k*-ω, based on the Wilcox model [13], is very sensitive to free stream values outside the shear layer. Several studies and applications have shown its efficiency in case of high flow pressure gradients. It is a two equations model; one for the turbulent kinetic energy *k* and other for the rate of turbulent dissipation energy ω.

The original equations of SST *k*-ω model are given by Eqs. (8) and (9):

$$\rho\frac{\partial k}{\partial t} + \rho u_j\frac{\partial k}{\partial x_j} = P - \beta^*\rho\omega k + \frac{\partial}{\partial x_j}\left[(\mu + \sigma_k\mu_t)\frac{\partial k}{\partial x_j}\right] \quad (8)$$

$$\rho\frac{\partial \omega}{\partial t} + \rho u_j\frac{\partial \omega}{\partial x_j} = \frac{\gamma\omega}{k}P - \beta\rho\omega^2 + \frac{\partial}{\partial x_j}\left[(\mu + \sigma_\omega\mu_t)\frac{\partial k}{\partial x_j}\right] + 2(1-F_1)\frac{\rho\sigma_{\omega_2}}{\omega}\frac{\partial k}{\partial x_i}\frac{\partial \omega}{\partial x_i} \quad (9)$$

where,

$$P = \tau_{ij}\frac{\partial u_i}{\partial x_j} \quad , \quad \gamma_1 = \frac{\beta_1}{\beta^*} - \frac{\sigma_{\omega_1}k^2}{\sqrt{\beta^*}} \quad \text{and} \quad \gamma_2 = \frac{\beta_2}{\beta^*} - \frac{\sigma_{\omega_2}k^2}{\sqrt{\beta^*}}$$

F_1 = 1 inside the boundary layer and 0 in the free stream.

The constants appeared in above equations are given in Table 1:

Table 1. Constants for SST *k*-ω turbulence model.

β^*	β_1	β_2	σ_{k1}	σ_{k2}	$\sigma_{\omega 1}$	$\sigma_{\omega 2}$	γ_1	γ_2	k
0.09	0.075	0.0828	0.85	1	0.5	0.856	0.5532	0.4404	0.41

3. Mesh Topology

The CFD approach is used to predict the aerodynamic performances of horizontal axis wind turbine for S809 airfoil. It provides a good precision to investigate effects of the mesh refinement and the boundary layer on the obtained results. Generally, a numerical solution becomes more precise with mesh refinement, but using the additional grids also increases the required memory and computing time.

The appropriate number of grids can be increased until the mesh is sufficiently fine so that further refinement does not change the results.

The mesh quality and the domain size in the CFD calculation directly influence on the computation accuracy and the convergence time. A good mesh should be large enough to avoid boundary effects, there are many types of meshes in CFD simulation the flow around airfoil wind turbine. The most popular mesh topology is the C-type mesh, which is designed to have a C-type topology around the airfoil. The dimensions of computational domain must be sufficient to predict the turbulence phenomenon, pressure and velocity distribution, then the domain size must be studied accurately. Domain size as shown in Fig. 2 is generated using ANSYS/WORKBENCH, the airfoil is located in the centre of a computational domain that extends to a distance of 6 times the chord length, in all directions from the airfoil aerodynamic centre, except at the wake, the airfoil is located of 11 times chord length to correctly reproduce the wake effect.

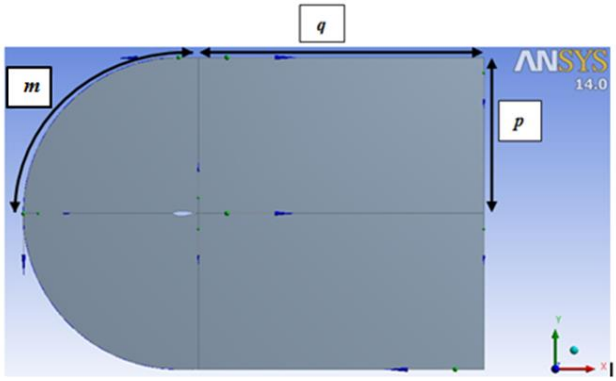

Fig. 2. Geometry and dimensions of computational domain.

The domain discretization was made using a structured quadrilateral mesh, as illustrated in Fig. 3.

The 2D mesh is a structured C-type generated. The mesh contains 183816 grids with 300 grids around the airfoil surface, 150 grids normal to airfoil surface and 250 grids extending from trailing edge. The refinement is very condensed near the airfoil surface in order to enclose the boundary layer approach, a large number of grids around the airfoil surface are used to capture the pressure gradient accurately.

In the near-airfoil region, a suitable resolution of the mesh in the orthogonal direction to the solid walls is conventionally recommended to compute the boundary layer airfoil (y^+). In this work, we used the advanced SST k-ω

turbulence model of Menter, it need a very fine mesh near the wall with y^+ values essentially lower than one as shown in Fig. 4 required by k-ω turbulence model.

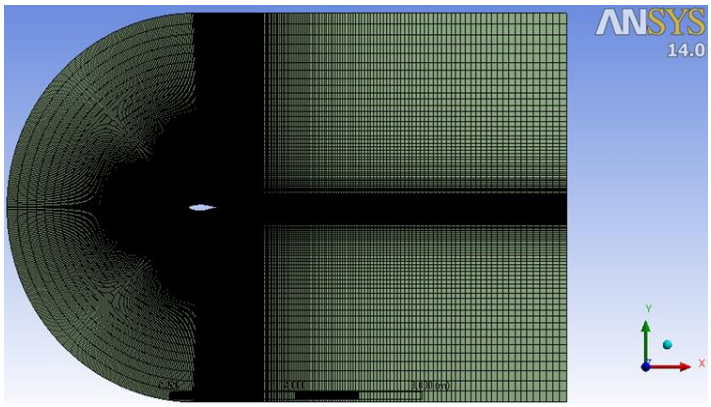

Fig. 3. Structured mesh area.

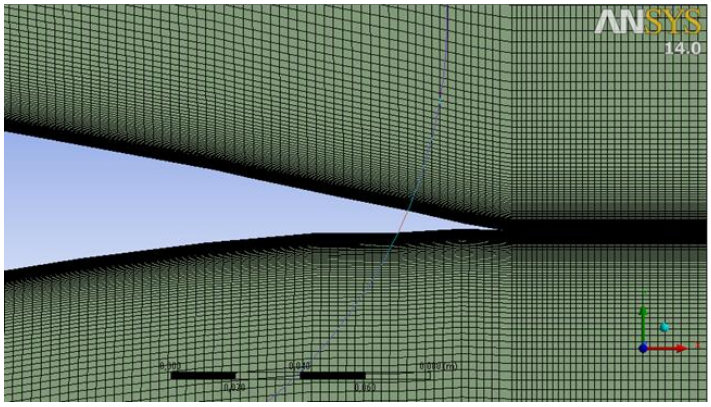

Fig. 4. Mesh around trailing edge.

In order to satisfy the SST k-ω turbulence model limitations must be $y^+<1$ was obtained and defined by Eq. (10).

$$y^+ = yu^* / \upsilon \tag{10}$$

where y is the distance of the first grid point from the rotor, u^* is the friction velocity.

It is possible to get a first attempt value of y by imposing $y^+ < 1$ in Eq. (11)

$$y = \frac{\upsilon y^+}{u^*} \tag{11}$$

By substituting $y^+=1$ in Eq. (11) gives $y=2.35*10^{-5}$ m.

where $u^* = \sqrt{\frac{\tau_p}{\rho}}$

4. Boundary Conditions

The boundary conditions have a significant influence on the results of simulation. In the present work, the velocity components at the inflow boundary are calculated based on the desired Reynolds number and chord length, the pressure is restricted to the zero-gradient condition. All these parameters given in Table 2 are used in FLUENT.

Table 2. Fluent parameters.

Turbulence model	k-ω SST
Fluid	Air, incompressible, unsteady
Density (ρ)	1.225
Dynamic viscosity (μ)	1.7894×10^{-5}
Turbulence Intensity	2.84%
Inlet velocity V_∞	14.6
Atmospheric pressure (P_{atm})	101325
Chord length (c)	1
Discretization scheme	Pressure (second order upwind) Momentum (second order upwind)
Reynolds number	10^6
CFD algorithm	Coupled

The velocity components along x and y directions are calculated as follow: $V_x = V_\infty \cos\alpha$ and $V_y = V_\infty \sin\alpha$, where α is angle of attack.

The free stream velocity V_∞=14.6 m/s based on Reynolds number equals to 10^6. No-Slip boundary conditions are applied along the airfoil surface, and at the outflow boundary, the ambient atmospheric pressure condition is applied and the velocity is set to the zero-gradient condition.

The inlet turbulence intensity is set to the level of 2.84%, the free stream temperature is 288.15 K, which is same as the environmental temperature and hydraulic diameter D_h is equal to the chord length 1 m. FLUENT solver uses a finite volume method to solve the Reynolds Averaged Navier-Stokes equations. Furthermore, pressure based solver COUPLED was used as the pressure-velocity coupling algorithm, and the discretization of turbulence model equations k-ω was made using the diagram second order upwind. For obtained height precisions, the convergence criterions for the absolute residuals of equation variables are set below 10^{-5}.

5. Results and Discussions

A grid independency study is performed by refining the mesh around the airfoil surface and increasing the number of grids in the streamwise and normal directions represented by geometric parameters m, p and q given by Table 3.

Table 3. Lift and drag coefficients for four meshes refinement.

Mesh number	*m, p, q* parameters size	Number of grids	y^+
Mesh 1	m =50, p =75, q =150	61716	0.93
Mesh 2	m =100, p =100, q =200	113058	0.81
Mesh 3	m =100, p =150, q =250	183816	0.7
Mesh 4	m =100 p =200, q =300	264374	0.65

The lift and drag coefficients presented in Figs. 5 and 6 are calculated for different meshes size at each angle of attack 0°, 6.16°, 8.2°, 10.2°, 12.23° and 14.23°.

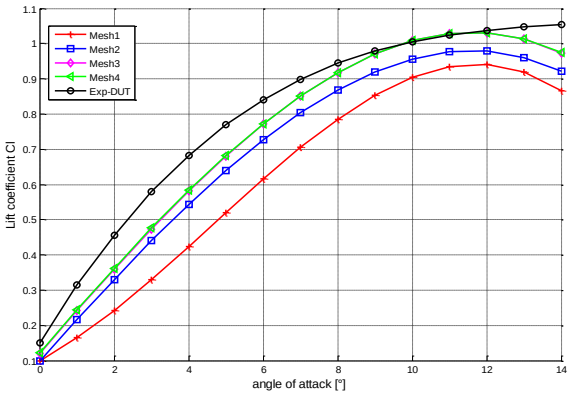

Fig. 5. Lift coefficient for different meshes size as a function of angle of attack for Re=10^6.

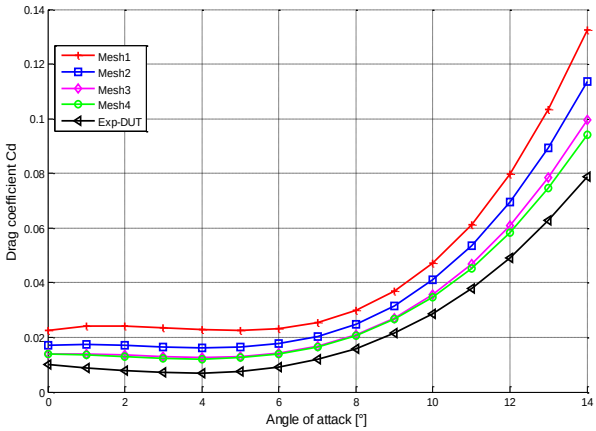

Fig. 6. Drag coefficient for four meshes size as a function of angle of attack for Re=10^6.

Figures 5 and 6 show the effect of number grids on lift and drag coefficients at different angles of attack. This study has revealed that the meshes 3 and 4 have the same results at stall angle and are in good agreement with the experimental data. To this point the results becomes independent with the number grids. Therefore, we choose the mesh 3, which gives best results with a minimum calculation time.

Table 4 presents the lift coefficient and dimensionless wall y^+ values for different meshes sizes. The table shows that the lift coefficient obtained by the meshes 3 and 4 is greater than those obtained by the meshes 1 and 2 because the mesh refinement around the airfoil surface is very fine and have the values of y^+ are less than one and converge to 0, which makes to solve the problem of boundary layer. We concluded that the results obtained by the SST k-ω turbulence model are very sensitive to the resolution of the boundary layer. Using SST k-ω

turbulence model, the value of y^+ must be less than 1 for the first grid mesh around airfoil surface (y_0=2.5×10^{-5} m), y_o is the distance between airfoil surface and middle of first grid.

Table 4. Dimensionless wall *y*+ and lift coefficient Cl distribution versus number of grid at angle of attack 6.16°.

	Number of grids	y^+	C_l
Mesh 1	61716	0.93	0.62
Mesh 2	113058	0.81	0.73
Mesh 3	183816	0.7	0.77
Mesh 4	264374	0.65	0.77

Figure 7 shows that at low angles of attack, the dimensionless lift coefficient increased linearly with attack angle. Flow was attached to the airfoil throughout this regime. At angle of attack roughly 15° to 16°, the flow on the upper surface of airfoil began to separate and a condition known as stall began to develop. The meshes 4, 3 and 2 have a good agreement with the experimental data and the same behaviour until angle of attack 8°.

The numerical results of drag coefficient presented in Fig. 8 shows that less than 5% error between numerical and experimental results when the angle of attack is less than 12° and the C_d curve is slowly increase, after this angle the error increases with increases angle of attack and C_d increases rapidly, this phenomenon is called stall, and this critical angle of attack is called stall angle.

At higher values of α, the results of our work don't in accordance with experimental data, because the flow can no longer follow the upper surface of the airfoil and becomes detached. There is a region above the upper surface, near the trailing edge, where the velocity is low and the flow reverses direction in places in a turbulent motion. This phenomenon is trailing edge separation. As the angle of attack is increased further, the beginning of the region of separated flow moves towards the leading edge of the airfoil. At a critical angle of attack, the lift component of the aerodynamic force falls off rapidly and the drag component increases rapidly.

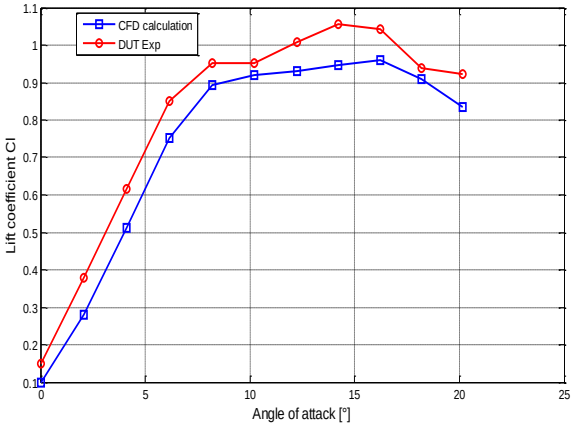

Fig. 7. Lift coefficient variation versus angle of attack for Re=10^6.

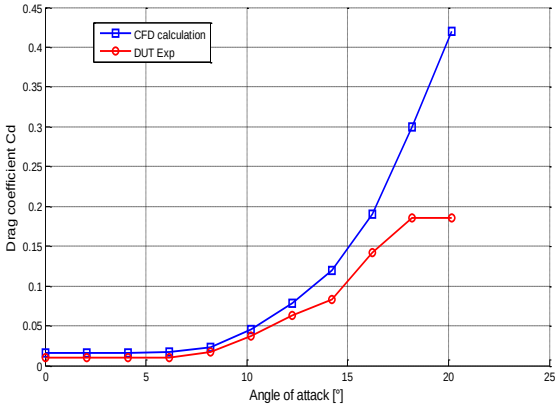

Fig. 8. Drag coefficient variation versus angle of attack for Re=10^6.

6. Conclusions

The flow analysis around a wind turbine airfoil has been carried out using the unsteady incompressible Reynolds Averaged Navier-Stokes equations. For studying boundary layer and mesh refinement, four meshes are compared. The lift and drag coefficients are calculated for each angle of attack.

The calculation showed that the mesh refinement in area boundary layer has a significant effect on the results quality, in particular the lift and drag coefficients, which have direct consequences on the aerodynamic performance of S809 airfoil.

The C_l/C_d ratio increase with increasing the angle of attack up to 6.5°, after that decrease, this angle called optimal angle of attack.

References

1. Swanson, R.C.; and Langer, S. (2016). Steady-state laminar flow solutions for NACA 0012 airfoil. *Computers and Fluids*, 126, 102-128.
2. Zhou, L.; Yunjun, Y.; Anlong, G.; and Weijiang, Z. (2015). Unstructured adaptive grid refinement for flow feature capture. *2014 Asia-Pacific International Symposium on Aerospace Technology*, 99, 477-483.
3. Bekhti, A.; and Guerri, O. (2012). Influence de la rugosité sur les caractéristiques aérodynamiques d'un profil de pale d'éolienne. *Revue des Energies Renouvelables*, 15(2), 235-247.
4. Moshfeghi, M.; Song, Y.J.; and Xie, Y.H. (2012). Effects of near-wall grid spacing on SST *k-ω* model using NREL Phase VI horizontal axis wind turbine. *Journal of Wind Engineering and Industrial Aerodynamics*, 107-108, 94-105.
5. Genç, M.S.; Karasu, I.; and Açıkel, H.H. (2012). An experimental study on aerodynamics of NACA2415 aerofoil at low Re numbers. *Experimental Thermal and Fluid Science*, 39, 252–264.

6. Kapsalis, P.C.S.; Voutsinas, S.; and Vlachos, N.S. (2016). Comparing the effect of three transition models on the CFD predictions of a NACA0012 airfoil aerodynamics. *Journal of Wind Engineering and Industrial Aerodynamics,* 157, 158–170.
7. Guerri, O.; Bouhadef, K.; and Harhad, A. (2006). Turbulent flow simulation of the NREL S809 Airfoil. *Wind engineering*, 30(4), 287-302.
8. Eleni, D.C.; Athanasios, T.I.; and Dionissios, M.P. (2012). Evaluation of the turbulence models for the simulation of the flow over a National Advisory Committee for Aeronautics (NACA) 0012 airfoil. *Journal of Mechanical Engineering Research*, 4, 100-111.
9. Bai, C.J.; Hsiao, F.B.; Li, M.H.; Huang, G.Y.; and Chen, Y.G. (2013). Design of 10 kW horizontal-axis wind turbine (HAWT) blade and aerodynamic investigation using numerical simulation. *7th Asian-Pacific Conference on Aerospace Technology and Science*, 67, 279-287.
10. Song, Y.; Perot, J.B. (2015). CFD Simulation of the NREL Phase VI rotor. *Wind Engineering*, 39(3), 299-310.
11. Sayed, M.A.; Kandil, H.A.; and A. Shaltot (2012). Aerodynamic analysis of different wind-turbine-blade profiles using finite-volume method. *Energy Conversion and Management*, 64, 541-550.
12. Menter, F.R. (1994). Two-equation eddy-viscosity turbulence models for engineering applications. *AIAA Journal*, 32(8), 1598-1605.
13. Wilcox, D.C. (2008). Formulation of the k-omega turbulence model revisited. *AIAA Journal*, 46(11), 2823-2838.